

pubs.acs.org/JPCC Article

Complex Dependence of Optoelectronic Properties of Metal Halide Perovskite Thin Films on Quantum Dot Decoration Layers

Published as part of The Journal of Physical Chemistry C virtual special issue "The Physical Chemistry of Perovskites".

Jorge Arteaga, Vivien Cherrette, Jin Zhong Zhang,* and Sayantani Ghosh*



Cite This: *J. Phys. Chem. C* 2023, 127, 17836–17842



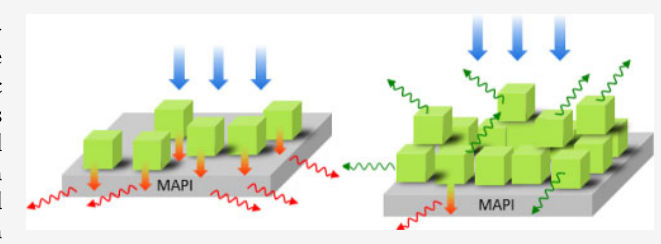
ACCESS

III Metrics & More

Article Recommendations

s Supporting Information

ABSTRACT: The interaction between CH₃NH₃PbI₃ (methylammonium lead iodide or MAPI) thin films and metal halide perovskite quantum dots (PQDs) was studied using spectroscopic techniques. By comparing PQDs with Cs⁺ and CH₃NH₃⁺ cations and different surface passivation, including both conducting and insulating molecular ligands, charge transfer interactions between the PQDs and the MAPI films were tuned. Mapping static and dynamic MAPI emission as functions of temperature, excitation wavelength, and excitation power revealed that a low density of



PQDs improved MAPI photoluminescence (PL) properties, including increased intensity and average recombination lifetime. However, a high density of PQDs had detrimental effects, resulting in a spectral blue shift of MAPI emission and a shortening of charge carrier lifetimes. This complex modulation of MAPI properties by PQDs indicates an intricate interplay between different factors that need to be considered in optimizing such heterostructures for optoelectronic applications.

1. INTRODUCTION

Metal halide perovskites (MHPs) are at the forefront of materials research owing to their superior optical and electronic properties¹⁻³ which have led to their utilization in a broad range of applications. These include photovoltaics, 4,5 light-emitting diodes, luminescent solar concentrators, lasers,8 and photodetectors.9 MHPs have an ABX3 crystal structure, where A is a monovalent cation (common examples include methylammonium, formamidinium, or Cs), B is a bivalent cation (Pb2+ or Sn2+), and X is a halide (Cl-, Br-, or I⁻).² Synthesis of MHPs with mixtures of A and X is a common approach 10 in the ongoing efforts to improve material quality and optoelectronic properties. Another strategy is to passivate the surface of MHP thin films, ¹¹⁻¹⁴ which serves a dual purpose of passivating defects ¹⁵ and reducing ion migration. ¹⁶ Passivation of defects, especially at grain boundaries, reduces non-radiative recombination losses, enhances overall charge carrier lifetimes, and increases charge extraction efficiency. 15 Reducing ion migration through defect centers improves MHP stability related to chemical degradation, which is particularly important when the A cation is an organic one. 16-18

Interactions between perovskite quantum dots (PQDs) and MHP thin films are of strong interest as PQDs with tunable properties can be used to modify and enhance the properties of the films. 15,16,19–22 While other QDs, such as CdSe and PbS, 19,21 have been studied for this purpose, PQDs are unique

candidates due to their similarity in properties to MHP films^{23–25} and have demonstrated the highest potential. PQDs can be integrated into thin film devices in two ways: as a thin decoration layer on top²⁶ using various deposition techniques such as spin coating,^{13,20} drop casting,²⁶ or spray coating²⁷ or as a dispersed layer within the bulk of the film, using techniques such as sol–gel,²⁸ co-precipitation,²⁵ or hydrothermal²⁰ methods. The use of both all-inorganic¹⁶ and organic–inorganic hybrid¹⁷ PQDs has led to favorable outcomes when incorporated into MHP films. These include improved stability of the thin films to environmental factors such as moisture and oxygen by virtue of defect annealing,²⁴ enhanced light harvesting efficiency by trapping the incident light within the film and improving the charge transport and extraction properties by increasing grain sizes,¹⁶ reducing recombination rates,²⁵ and enhancing higher optical yield.²³

In this work, PQDs of varying composition, surface functionalization, and coverage density were deposited on CH₃NH₃PbI₃ (methylammonium lead iodide, known as MAPI) thin films to study how different material parameters

Received: June 6, 2023 Revised: August 11, 2023 Published: August 29, 2023





affect MAPI optoelectronic properties from a spectroscopic perspective and as a function of temperature. The results suggest a complex dependence of the interactions between the QDs and MAPI films on the characteristics of the PQDs and the coverage of the PQDs on the surface of the MAPI films.

2. EXPERIMENTAL SECTION

- **2.1. Chemicals.** Methylammonium iodide (MAI, \geq 99%, Sigma-Aldrich), lead iodide (PbI₂, 99%, Sigma-Aldrich), *N*-methyl-2-pyrrolidone (NMP, 99.5%, Sigma-Aldrich), dimethyl sulfoxide (DMSO, \geq 99.9%, Sigma-Aldrich), *N*,*N*-dimethylformamide (DMF, 99.8%, Sigma-Aldrich), and cesium lead bromide PQDs (CsPbBr₃, 10 mg/mL, Sigma-Aldrich) were used as purchased without any further purification.
- **2.2. Synthesis.** For thin film fabrication, MAPI ink was prepared in a glovebox. In a glass container, 0.636 g of MAI was combined with 1.844 g of PbI₂. Next, 68 μL of NMP, 232 μ L of DMSO, and 3 mL of DMF were added, and the ink was left to mix at 60 °C overnight. 40 µL of this MAPI ink was deposited on the substrates which had been cleaned with isopropyl alcohol and spin-coated at 2000 rpm for 60 s. This was followed by annealing the film at 100 °C for 5 min. For PQD deposition, the MAPI thin film was placed back in the spin coater, where 40 μ L of PQDs (all suspended in toluene) was deposited and spin-coated at 2000 rpm for 60 s, and the annealing process was repeated. For the density calculation of each type of PQD, molar concentration was used as the starting point. As an example, MA-APTES PQDs had a molar concentration of 3.00 mM/L. This led to 40 μ L containing 8 \times 10¹⁶ dots. Calculations²⁹ were used to estimate that 0.038 fractions of the PQDs were deposited on the film after spin coating. Over the entire substrate, this amounted to 1.6×10^7 $dots/\mu m^2$. The same calculation for Cs-OABr PQDs led to 0.8 $\times 10^8$ dots/ μ m² and MA-BZA/PAA to 2.7×10^7 dots/ μ m².
- **2.3. Characterization.** 2.3.1. Spectroscopy. The samples were excited by a pulsed supercontinuum source (NKT Photonics), which allowed spectral selection and modulation of the pulse interval. Most of the PL (static and dynamic) data were taken with this source tuned to 430 or 620 nm and 76 MHz repetition rate using a Princeton Instruments Acton SP2300 spectrometer, which dispersed the emission onto a thermo-electrically cooled charged coupled detector. The spectral resolution of this system was 0.18 nm. For time-resolved measurements, the collected PL signal was directed to single-photon avalanche diodes that connect to a time-correlated single-photon counting system (PicoQuant).
- 2.3.2. Temperature-Dependent Measurements. The samples were mounted in a cryo-free optical system from Advanced Research Systems with an operation range of 295–6 K. Samples were mounted on a scanning stage with motorized micrometers along all three directions. The scanning stages had a spatial resolution of 100 nm.
- 2.3.3. Imaging. The confocal data was taken using an LSM880 confocal microscope. Samples were excited at 458 and at 633 nm above and below the PQDs' band gap. The emission was taken by filtering light between 469 and 526 nm for the PQD emission and between 708 and 759 nm for the MAPI emission.

3. RESULTS AND DISCUSSION

Figure 1A schematically summarizes the three different samples used. Two were CH₃NH₃PbBr₃ PQDs, one type

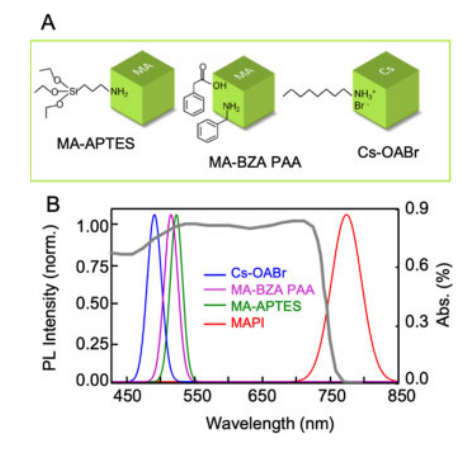


Figure 1. (A) Schematic of PQDs and molecules used to functionalize their surfaces: (left) CH₃NH₃PbBr₃ with APTES, (middle) CH₃NH₃PbBr₃ with BZA PAA, and (right) CsPbBr₃ with OABr. (B) Normalized PL spectra of the three PQDs in solution and PL and absorption bands of the MAPI film showing PQD emission overlap with MAPI absorption.

functionalized with 3-aminopropyl triethoxysilane, denoted MA-APTES, and the other with ligands containing benzylamine (BZA) and phenylacetic acid (PAA), denoted MA-BZA PAA. Both MA-APTES and MA-BZA PAA PQDs were synthesized following the protocols in our previous works. 29,30 The third PQD was CsPbBr3 functionalized with octylammonium bromide, labeled Cs-OABr, purchased from Sigma-Aldrich. Figure 1B shows the normalized photoluminescence (PL) spectra of each of the PQDs in solution, compared to PL emission from the MAPI film, with all the PQDs emitting at shorter wavelengths than the MAPI film. This was a deliberate choice to allow for the possibility of energy transfer from the larger band gaps of the PQDs to the smaller band gap of the film,³¹ given the spectral overlap between MAPI absorption and PQD emission bands. In addition, BZA PAA ligands are conductive and were chosen as an alternative to the insulating APTES and OABr ligands to allow for more efficient charge transfer from PQDs to films.

MAPI thin films were fabricated via spin coating and annealing, followed by the same procedure for PQD deposition. Calculations from the literature based on molar concentration revealed the density of PQDs to range between 10^7 and 10^8 dots/ μ m², which is well below the limit of a single close-packed PQD layer ($\sim 10^{10} \text{ dots/}\mu\text{m}^2$) and should not lead to inter-dot ET-induced spectral red-shift.³¹ These samples were denoted LD (low density), and another set, prepared with a second spin-coated deposition of the same concentration of PQD, was denoted high density (HD). Schematic representations of LD and HD films are shown in Figure 2A. Scanning electron microscopy (SEM) and X-ray photoelectron spectroscopy (XPS) (Figures S1 and S2) confirm no unexpected differences between the films. Figure 2B-F shows fluorescence confocal images of a MAPI film as it went through successive PQD depositions. Bare MAPI emission (Figure 2B) with 633 nm, when compared to those after the first PQD deposition (LD film, Figure 2C) and after the second (HD film, Figure 2E), showed no noticeable variation, indicating that the deposition and annealing did not cause significant changes to the film. The same film with excitation tuned to 458 nm (which excited both the PQDs and

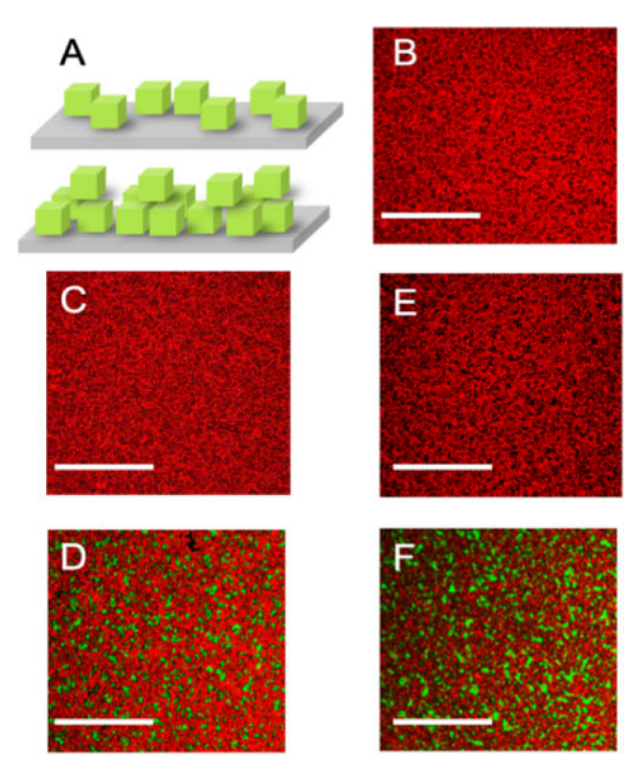


Figure 2. (A) Schematics of (top) LD and (bottom) HD films. (B) Confocal image of bare MAPI film. Images of the LD film taken with (C) 633 and (D) 458 nm excitation. Images of the HD film taken with (E) 633 and (F) 458 nm excitation. All images are of the same film taken after successive depositions. All scale bars are 250 μm.

MAPI) is shown in Figure 2D,F, highlighting the changes in PQD area coverage between LD and HD films.

Room-temperature PL results are summarized for all LD films in Figure 3. PL data were collected from, and averaged over, spatially resolved maps (Figure S3), and the resultant spectra in Figure 3A show that PQD emission was quenched for all the LD films, regardless of PQD composition or surface functionalization. For all thin films, MAPI emission was

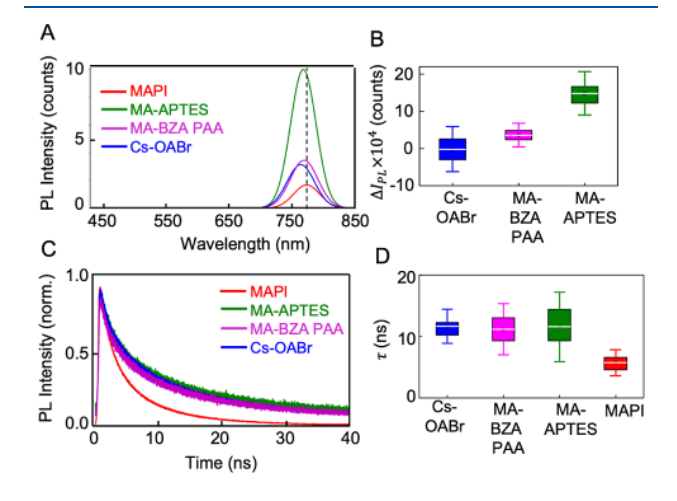


Figure 3. (A) PL emission of LD MAPI films shows quenched emission from the PQDs. (B) Change in PL intensity of the MAPI films with PQDs added (C) TRPL data for the same samples. (D) Distribution of average recombination lifetime τ for MAPI w/o PQDs and with. Addition of PQDs results in increased τ . Bars in (C and D) indicate the standard deviations.

recorded before and after PQD deposition. The same results also indicated a small blue shift (~5-10 nm, Figure S4A) of MAPI PL after PQD deposition, with enhanced intensity. This was investigated further in Figure 3B where MAPI PL intensity changes (ΔI_{PL}) for multiple samples are plotted. These confirm that overall, both MA-PQDs increased MAPI emission, while MA-APTES demonstrated nearly a threefold enhancement. Furthermore, compared to bare MAPI, the deposition of Cs-OABr and MA-BZA PAA PQDs increased spectral full width at half-maximum (FWHM) by a couple of nm, while MA-APTES PQDs led to narrower spectral widths in a large proportion of samples (Figure S2B). FWHM is an indicator of the quality of MAPI thin films and the presence of defects.³² Narrow FWHM values are associated with higher power conversion efficiency of solar cells.³³ Figure 3C juxtaposes time-resolved PL (TRPL) profiles of MAPI films with and without PQDs, and the former all demonstrated longer lifetimes. The TRPL decay profiles were fitted with a biexponential function, $I_{\rm PL} = A_1 {\rm e}^{-t/\tau_1} + A_2 {\rm e}^{-t/\tau_2}$, and the average recombination time was extracted using the weighted formula $\tau = (A_1 \tau_1^2 + A_2 \tau_2^2)/(A_1 \tau_1 + A_2 \tau_2)^{34}$ Compiled from multiple samplings, Figure 3D confirms that τ was longer with the addition of all the PQDs.

The measurements were repeated with a second set of freshly made MAPI films, but with PQDs spin-coated twice, each time the same amount as before, denoted HD films. PQD PL was observed alongside MAPI for all three samples (Figure 4A–C). While the PL of the PQDs was not quenched by

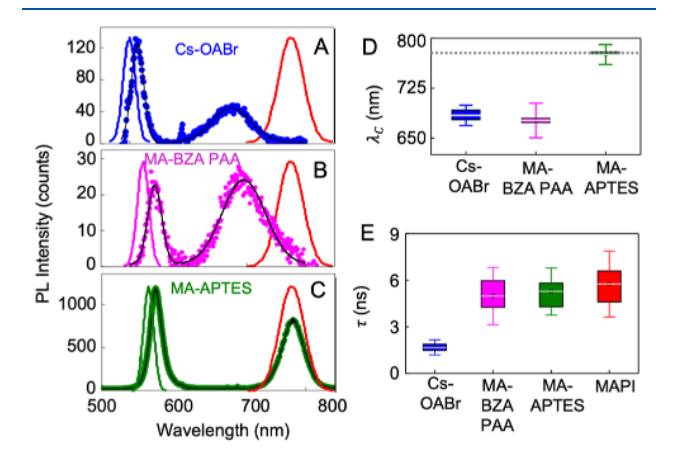


Figure 4. PL emission of MAPI films with HD of (A) CsPbBr₃ PQDs with OABr, (B) CH₃NH₃PbBr₃ PQDs with BZA/PAA, and (C) CH₃NH₃PbBr₃ PQDs with APTES, showing emission from both MAPI and the QDs. The red curve indicates bare MAPI emission, while the solid curves in each plot indicate PQD emission in solution. (D) Center wavelength $\lambda_{\rm C}$ of MAPI emission with the PQDs. The dashed line indicates the peak position of the bare MAPI film. (E) Distribution of average recombination lifetime τ for MAPI w/o PQDs and with. The bars in (D) and (E) indicate the standard deviations.

MAPI, its peak position red-shifted by 15–20 nm compared to solution PL, attributed to inter-dot energy transfer. MAPI PL from films with Cs-OABr (Figure 4A) and MA-BZA PAA (Figure 4B) was blue-shifted by nearly 100 nm, and the spectra were notably broadened (Figure S5). MA-APTES PQDs (Figure 4C) proved to be an exception to the blue shift, as further summarized in Figure 4D. Recombination lifetimes extracted from TRPL data as plotted in Figure 4E did not show any increase for MA-APTES and a minor decrease for MA-

BZA PAA. But Cs-OABr PQDs suppressed τ on average by almost half.

PL properties, including emission intensity, wavelength, and recombination rates, are usually affected by a combination of mechanisms. One is the passivation of surface traps that reduce non-radiative recombination, leading to enhanced PL intensity and decreased spectral FWHM¹⁵ observed in LD films (Figure S6). APTES is a well-known passivation agent, 30,35 and BZA PAA can neutralize dangling bonds,³⁶ reducing non-radiative recombination. The other is energy transfer (ET) from PQDs to MAPI, which can also increase emission efficiency and charge carrier lifetimes in the acceptor (entity with a lower bandgap).³⁷ There is a third possibility, where the annealing process following PQD deposition leads to ions being released from them to neutralize halide vacancies.³⁸ In addition to passivation of specific defects, this could lead to the formation of localized domains of CH3NH3PbI3-vBrv, causing the spectral blue shift observed in Figures 3A and 4D and the reduced recombination in Figure 4E.

Variations of excitation wavelength and temperature revealed further differences between the PQDs and their effect on MAPI. Figure 5A,B schematically outlines the role of

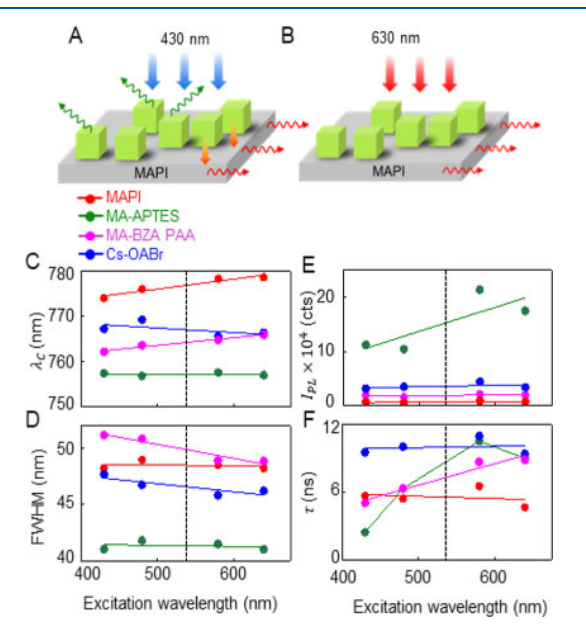


Figure 5. Schematics indicating the consequences of exciting (A) above and (B) below the band gap of PQDs. (C) Center emission wavelength $\lambda_{\rm C}$, (D) FWHM, and (E) average recombination time τ of MAPI emission with and without PQDs as the excitation wavelength is tuned. The dashed line indicates the wavelength below which both PQDs and MAPI are excited.

excitation wavelength. When both PQDs and MAPI were excited (430 nm below PQD bandgaps), emission from each was expected, and there was a likelihood of ET from PQD to MAPI. If the excitation wavelength was longer (630 nm) and the PQDs were not excited, the only photophysical process would be direct absorption by and emission from MAPI. In Figure 5C–F, MAPI emission wavelength $\lambda_{\rm C}$, spectral FWHM, emission intensity $I_{\rm PL}$, and average recombination time τ are plotted as the excitation wavelength was tuned from 430 to 650 nm for LD films. $\lambda_{\rm C}$ and FWHM did not show any consistent and noteworthy variation with the excitation wavelength. ET may not necessarily have affected those

parameters but changes to $I_{\rm PL}$ and τ were expected. For films with MA-BZA PAA and Cs-OABr, there were no changes in $I_{\rm PL}$ (Figure 5E). Films with MA-APTES did indicate an increase in excitation wavelength. Similarly, both MA-APTES and MA-BZA PAA incorporated MAPI films showed τ increasing at longer excitation wavelengths. If ET from the PQDs was the cause, then both $I_{\rm PL}$ and τ should have been enhanced for excitation <500 nm when carriers were excited in the PQDs. The reverse was noticed, and therefore, it leads to the conclusion that ET does not play a critical role in the trends observed.

All MAPbX₃ undergoes a structural phase transition as temperature is decreased. For MAPI, for T > 140 K, the crystal structure is tetragonal with a bandgap of 1.56 eV (\sim 790 nm), after which the system stabilizes in an orthorhombic structure with a higher bandgap at 1.62 eV (~760 nm).39 As the temperature of the MAPI films was changed from 300 to 6 K, the expected phase transition was observed in all samples (Figure S7A-D),³⁹ though the spectral shifts indicate retention of tetragonal domains in films with PQDs (Figure S7E-G). Strain at surfaces/interfaces is a common cause of such an effect, 40 and the energy of emission at neither phase is affected. Plotting MAPI lifetime τ versus temperature for films with all three PQD in Figure 6A shows that τ increased with temperature T in all cases, which is typical of MAPI and implies that recombination is dominated by excitons rather than free charges.40

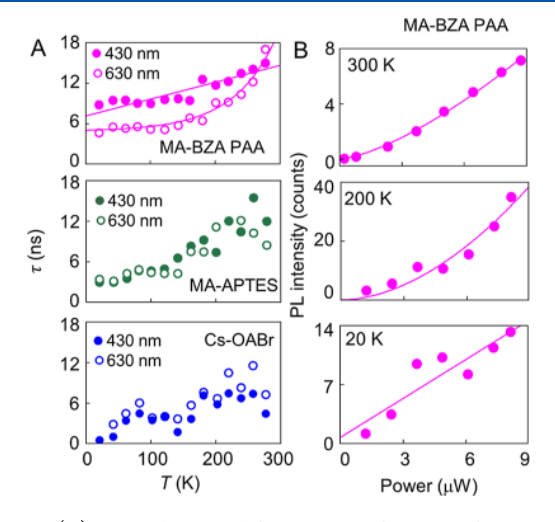


Figure 6. (A) Recombination lifetime τ as a function of temperature T for two different excitation wavelengths for (top) CH₃NH₃PbBr₃ with BZA/PAA, (middle) CH₃NH₃PbBr₃ with APTES, and (bottom) CsPbBr₃ with OABr. (B) PL intensity varying with MAPI carrier density at T=300, 200, and 20 K for the same PQDs. Fits are to a power law.

For MA-APTES and Cs-OABr, excitation wavelength did not affect lifetime, but τ was consistently higher in the MAPI film for 430 nm excitation for samples with MA-BZA PAA in the range T < 260 K. Having established that ET does not play a substantial role in modulating MAPI behavior, it is feasible that charge transfer from the MA-BZA PAA PQDs to MAPI, resulting from the higher conductivity afforded by the aromatic BZA PAA ligands compared to the insulating behavior of APTES and OABr. A final consequence of the deposition of PQDs with conducting ligands is seen in Figure 6B, which plots MAPI emission intensity $I_{\rm PL}$ with excitation power at 295,

200, and 20 K for an excitation wavelength of 430 nm. At 295 K, $I_{\rm PL} \propto P_{\rm exc} 2$, where $P_{\rm exc}$ is excitation power, which is indicative of free charge carrier recombination and was consistent for bare MAPI (Figure S8) and in MAPI with all three PQDs (Figures 6B, S9, and S10). At 20 K, $I_{\rm PL} \propto P_{\rm exc}$ for all samples, implying recombination is excitonic, as expected at low temperatures when the thermal energy is lower than the excitonic binding energy. However, at 200 K, MAPI PL emission from films with MA-APTES and Cs-OABr PQDs showed a linear dependence with excitation power (Figures S9 and S10), while MAPI with MA-BZA PAA exhibited bimolecular recombination. Assuming there is no charge transfer from the other two types of PQDs, then the behavior of those MAPI films is the norm, leading to the conclusion that free charges from MA-BZA PAA PQDs result in this anomalous power dependence.

Taken together, these results showed complex changes in thin film optoelectronic properties, driven by three primary mechanisms, schematically depicted in Figure 7. At LD of

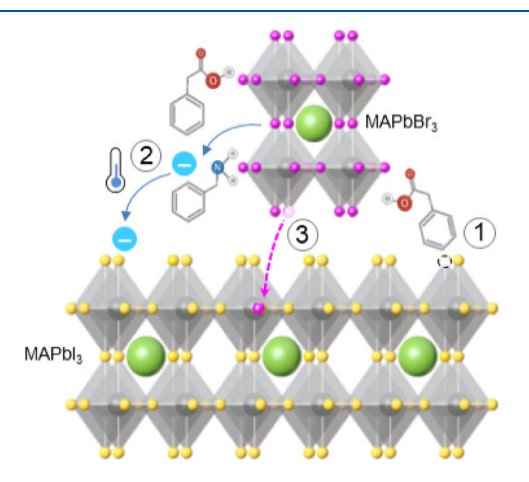


Figure 7. Schematic summarizing the most dominant effects observed between MAPI and the PQDs. (1) Passivation of vacancy-related dangling bonds in MAPI by some PQDs increases PL yield and improves recombination lifetimes; (2) at low temperatures (T < 200 K), PQDs with conducting ligands allow charge transfer to MAPI, increasing bimolecular recombination; and (3) halide ion migration from PQDs to MAPI results in spectral blue shift and increased recombination rates, particularly impactful in the HD films.

PQDs, MAPI surface defects were passivated, leading to increased emission intensity and improved recombination lifetimes. The role of surface ligands on the PQDs became clearer at lower temperatures, where the conducting BZA PAA molecules allowed for charge transfer, reflected in an increased charged lifetime and in an increased proportion of free carriers participating in recombination. There is also the possibility that the annealing process following PQD deposition led to ion migration and the formation of domains of I/Br mixed perovskite, and this consequence was more severe after the second annealing when the PQD density was doubled in the case of MA-BZA PAA and Cs-OABr PQDs. Ion migration in MAPbX₃ films is a well-established occurrence and has been investigated in depth in both thin films 42-49 and nanocrystals. 50,51 In particular, because the Pb-Br bond is shorter and stronger, 52-57 I is replaced by Br with relative ease, and this substitution can be driven optically⁵⁸ or thermally.⁵ Furthermore, the clearest indication of halide migration is a

spectral shift in PL, which extends between 100–125 nm in wavelength, 50,51,58 as we have observed here.

4. CONCLUSIONS

This study of MHP PQDs deposited on MAPI using spectroscopic techniques reveals the critical role of the surface and interfaces in MHP-based materials and provides some insights into how surface optimization may be attempted to achieve desired features for different applications. For higher PL emission yield, insulating bulky molecules are better, while in cases where conduction is a necessity, aromatic ligands may be more suited.

ASSOCIATED CONTENT

Supporting Information

The Supporting Information is available free of charge at https://pubs.acs.org/doi/10.1021/acs.jpcc.3c03832.

Example of spatially resolved PL data mapping for MAPI film with and without MA-APTES PQDs, distribution of PL emission spectra and FWHM for samples with and without PQDs at both low and high densities, comparison of recombination lifetimes and spectral FWHM for samples with PQDs at both high and low densities, temperature-dependent PL spectra for samples with PQDs, plot of PL intensity as a function of excitation power at 430 nm for MAPI and samples with MA-APTES and Cs-OABr PQDs, SEM and XPS characterization of bare MAPI films, and MAPI with Cs-OABr PQDs at both LD and HD (PDF)

AUTHOR INFORMATION

Corresponding Authors

Jin Zhong Zhang — Department of Chemistry and Biochemistry, University of California, Santa Cruz, California 95064, United States of America; ● orcid.org/ 0000-0003-3437-912X; Email: zhang@ucsc.edu

Sayantani Ghosh — Department of Physics, University of California, Merced, California 95343, United States of America; orcid.org/0000-0003-3440-7194; Email: sghosh@ucmerced.edu

Authors

Jorge Arteaga – Department of Physics, University of California, Merced, California 95343, United States of America

Vivien Cherrette – Department of Chemistry and Biochemistry, University of California, Santa Cruz, California 95064, United States of America

Complete contact information is available at: https://pubs.acs.org/10.1021/acs.jpcc.3c03832

Notes

The authors declare no competing financial interest.

ACKNOWLEDGMENTS

This work was supported by funding from NASA grant no. NNH18ZHA008CMIROG6R and NSF grant no. DGE-2125510 and CHE 1904547.

REFERENCES

- (1) Olaleru, S. A.; Kirui, J. K.; Wamwangi, D.; Roro, K. T.; Mwakikunga, B. Perovskite solar cells: The new epoch in photovoltaics. *Sol. Energy* **2020**, *196*, 295–309.
- (2) Grätzel, M. The Light and Shade of Perovskite Solar Cells. *Nat. Mater.* **2014**, *13*, 838–842.
- (3) Manser, J. S.; Christians, J. A.; Kamat, P. V. Intriguing Optoelectronic Properties of Metal Halide Perovskites. *Chem. Rev.* **2016**, *116*, 12956–13008.
- (4) Jung, H. S.; Park, N.-G. Perovskite Solar Cells: From Materials to Devices. *Small* **2015**, *11*, 10–25.
- (5) Best Research-Cell Efficiency ChartlPhotovoltaic Researchl. National Renewable Energy Laboratory. 2023, https://www.nrel.gov/pv/cell-efficiency.html (accessed May 13, 2023).
- (6) Wang, H. C.; Bao, Z.; Tsai, H. Y.; Tang, A. C.; Liu, R. S. Perovskite Quantum Dots and Their Application in Light-Emitting Diodes. *Small* **2018**, *14*, 1702433.
- (7) Meinardi, F.; Akkerman, Q. A.; Bruni, F.; Park, S.; Mauri, M.; Dang, Z.; Manna, L.; Brovelli, S. Doped Halide Perovskite Nanocrystals for Reabsorption-Free Luminescent Solar Concentrators. ACS Energy Lett. 2017, 2, 2368–2377.
- (8) Xing, G.; Mathews, N.; Lim, S. S.; Yantara, N.; Liu, X.; Sabba, D.; Grätzel, M.; Mhaisalkar, S.; Sum, T. C. Low-Temperature Solution-Processed Wavelength-Tunable Perovskites for Lasing. *Nat. Mater.* **2014**, *13*, 476–480.
- (9) Tian, W.; Zhou, H.; Li, L. Hybrid Organic-Inorganic Perovskite Photodetectors. *Small* **2017**, *13*, 1702107.
- (10) Colella, S.; Mosconi, E.; Fedeli, P.; Listorti, A.; Gazza, F.; Orlandi, F.; Ferro, P.; Besagni, T.; Rizzo, A.; Calestani, G.; et al. $MAPbI_{3-x}$ Cl_x Mixed Halide Perovskite for Hybrid Solar Cells: The Role of Chloride as Dopant on the Transport and Structural Properties. *Chem. Mater.* **2013**, 25, 4613–4618.
- (11) Lee, S.; Kim, D. B.; Yu, J. C.; Jang, C. H.; Park, J. H.; Lee, B. R.; Song, M. H. Versatile Defect Passivation Methods for Metal Halide Perovskite Materials and Their Application to Light-Emitting Devices. *Adv. Mater.* **2019**, *31*, 1805244.
- (12) Xue, J.; Wang, R.; Yang, Y. The Surface of Halide Perovskites from Nano to Bulk. *Nat. Rev. Mater.* **2020**, *5*, 809–827.
- (13) Long, M.; Zhang, T.; Zhu, H.; Li, G.; Wang, F.; Guo, W.; Chai, Y.; Chen, W.; Li, Q.; Wong, K. S.; et al. Textured CH₃NH₃PbI₃ Thin Film with Enhanced Stability for High Performance Perovskite Solar Cells. *Nano Energy* **2017**, *33*, 485–496.
- (14) Khorshidi, E.; Rezaei, B.; Blätte, D.; Buyruk, A.; Reus, M. A.; Hanisch, J.; Böller, B.; Müller-Buschbaum, P.; Ameri, T. Hydrophobic Graphene Quantum Dots for Defect Passivation and Enhanced Moisture Stability of CH₃NH₃PbI₃ Perovskite Solar Cells. *Sol. RRL* **2022**, *6*, 2270072.
- (15) Hu, L.; Duan, L.; Yao, Y.; Chen, W.; Zhou, Z.; Cazorla, C.; Lin, C.; Guan, X.; Geng, X.; Wang, F.; et al. Quantum Dot Passivation of Halide Perovskite Films with Reduced Defects, Suppressed Phase Segregation, and Enhanced Stability. Adv. Sci. 2022, 9, 2102258.
- (16) Wang, T.; Deng, W.; Cao, J.; Yan, F. Recent Progress on Heterojunction Engineering in Perovskite Solar Cells. *Adv. Energy Mater.* **2022**, 1–35, 2201436.
- (17) Yuan, Y.; Huang, J. Ion Migration in Organometal Trihalide Perovskite and Its Impact on Photovoltaic Efficiency and Stability. *Acc. Chem. Res.* **2016**, *49*, 286–293.
- (18) Rakshit, S.; Piatkowski, P.; Mora-Seró, I.; Douhal, A. Combining Perovskites and Quantum Dots: Synthesis, Characterization, and Applications in Solar Cells, LEDs, and Photodetectors. *Adv. Opt. Mater.* **2022**, *10*, 2102566.
- (19) Baronnier, J.; Houel, J.; Dujardin, C.; Kulzer, F.; Mahler, B. Doping MAPbBr₃ Hybrid Perovskites with CdSe/CdZnS Quantum Dots: From Emissive Thin Films to Hybrid Single-Photon Sources. *Nanoscale* **2022**, *14*, 5769–5781.
- (20) Chen, H.; Luo, Q.; Liu, T.; Tai, M.; Lin, J.; Murugadoss, V.; Lin, H.; Wang, J.; Guo, Z.; Wang, N. Boosting Multiple Interfaces by Co-Doped Graphene Quantum Dots for High Efficiency and

- Durability Perovskite Solar Cells. ACS Appl. Mater. Interfaces 2020, 12, 13941–13949.
- (21) Cao, Y.; Stavrinadis, A.; Lasanta, T.; So, D.; Konstantatos, G. The Role of Surface Passivation for Efficient and Photostable PbS Quantum Dot Solar Cells. *Nat. Energy* **2016**, *1*, 16035.
- (22) Que, M.; Dai, Z.; Yang, H.; Zhu, H.; Zong, Y.; Que, W.; Padture, N. P.; Zhou, Y.; Chen, O. Quantum-Dot-Induced Cesium-Rich Surface Imparts Enhanced Stability to Formamidinium Lead Iodide Perovskite Solar Cells. ACS Energy Lett. 2019, 4, 1970—1975.
- (23) Zheng, X.; Troughton, J.; Gasparini, N.; Lin, Y.; Wei, M.; Hou, Y.; Liu, J.; Song, K.; Chen, Z.; Yang, C.; et al. Quantum Dots Supply Bulk- and Surface-Passivation Agents for Efficient and Stable Perovskite Solar Cells. *Joule* **2019**, *3*, 1963–1976.
- (24) Cheng, F.; He, R.; Nie, S.; Zhang, C.; Yin, J.; Li, J.; Zheng, N.; Wu, B. Perovskite Quantum Dots as Multifunctional Interlayers in Perovskite Solar Cells with Dopant-Free Organic Hole Transporting Layers. *J. Am. Chem. Soc.* **2021**, *143*, 5855–5866.
- (25) Cheng, X.; Han, Y.; Cui, B. Fabrication Strategies and Optoelectronic Applications of Perovskite Heterostructures. *Adv. Opt. Mater.* **2022**, *10*, 2102224.
- (26) Liu, T.; Liu, X.; Chen, D.; Liu, Q.; Zuo, Y.; Guo, X.; Zheng, J.; liu, Z.; Xue, C.; Cheng, B. Drop-Casting CsPbBr₃ Perovskite Quantum Dots as down-Shifting Layer Enhancing the Ultraviolet Response of Silicon Avalanche Photodiode. *Appl. Phys. Lett.* **2021**, *119*, 153501.
- (27) Dai, S. W.; Hsu, B. W.; Chen, C. Y.; Lee, C. A.; Liu, H. Y.; Wang, H. F.; Huang, Y. C.; Wu, T. L.; Manikandan, A.; Ho, R. M.; et al. Perovskite Quantum Dots with Near Unity Solution and Neat-Film Photoluminescent Quantum Yield by Novel Spray Synthesis. *Adv. Mater.* **2018**, *30*, 1705532.
- (28) Chavan, R. D.; Wolska-Pietkiewicz, M.; Prochowicz, D.; Jędrzejewska, M.; Tavakoli, M. M.; Yadav, P.; Hong, C. K.; Lewiński, J. Organic Ligand-Free ZnO Quantum Dots for Efficient and Stable Perovskite Solar Cells. *Adv. Funct. Mater.* **2022**, 32, 2205909.
- (29) Delmas, W. G.; Vickers, E. T.; DiBenedetto, A. C.; Lum, C.; Hernandez, I. N.; Zhang, J. Z.; Ghosh, S. Modulating Charge Carrier Dynamics and Transfer via Surface Modifications in Organometallic Halide Perovskite Quantum Dots. *J. Phys. Chem. Lett.* **2020**, *11*, 7886–7892.
- (30) Luo, B.; Pu, Y. C.; Lindley, S. A.; Yang, Y.; Lu, L.; Li, Y.; Li, X.; Zhang, J. Z. Organolead Halide Perovskite Nanocrystals: Branched Capping Ligands Control Crystal Size and Stability. *Angew. Chem., Int. Ed.* **2016**, *55*, 8864–8868.
- (31) de Weerd, C.; Gomez, L.; Zhang, H.; Buma, W. J.; Nedelcu, G.; Kovalenko, M. V.; Gregorkiewicz, T. Energy Transfer between Inorganic Perovskite Nanocrystals. *J. Phys. Chem. C* **2016**, 120, 13310–13315.
- (32) Lee, J.; Koteles, E. S.; Vassell, M. O. Luminescence Linewidths of Excitons in GaAs Quantum Wells below 150 K. *Phys. Rev. B: Condens. Matter Mater. Phys.* **1986**, 33, 5512–5516.
- (33) Yang, Y.; Lu, H.; Feng, S.; Yang, L.; Dong, H.; Wang, J.; Tian, C.; Li, L.; Lu, H.; Jeong, J.; et al. Modulation of Perovskite Crystallization Processes towards Highly Efficient and Stable Perovskite Solar Cells with MXene Quantum Dot-Modified SnO₂. *Energy Environ. Sci.* **2021**, *14*, 3447–3454.
- (34) Delmas, W. G.; Vickers, E. T.; DiBenedetto, A. C.; Lum, C.; Hernandez, I. N.; Zhang, J. Z.; Ghosh, S. Modulating Charge Carrier Dynamics and Transfer via Surface Modifications in Organometallic Halide Perovskite Quantum Dots. *J. Phys. Chem. Lett.* **2020**, *11*, 7886–7892.
- (35) Sha, Y.; Bi, E.; Zhang, Y.; Ru, P.; Kong, W.; Zhang, P.; Yang, X.; Chen, H.; Han, L. A Scalable Integrated Dopant-Free Heterostructure to Stabilize Perovskite Solar Cell Modules. *Adv. Energy Mater.* **2021**, *11*, 2003301.
- (36) Liu, L.; Pan, K.; Xu, K.; Zhang, J. Z. Impact of Molecular Ligands in the Synthesis and Transformation between Metal Halide Perovskite Quantum Dots and Magic Sized Clusters. *ACS Phys. Chem.* **2022**, *2*, 156–170.

- (37) Kholmicheva, N.; Moroz, P.; Eckard, H.; Jensen, G.; Zamkov, M. Energy Transfer in Quantum Dot Solids. *ACS Energy Lett.* **2017**, *2*, 154–160.
- (38) Kong, W.; Ye, Z.; Qi, Z.; Zhang, B.; Wang, M.; Rahimi-Iman, A.; Wu, H. Characterization of an Abnormal Photoluminescence Behavior upon Crystal-Phase Transition of Perovskite CH₃NH₃PbI₃. *Phys. Chem. Chem. Phys.* **2015**, *17*, 16405–16411.
- (39) Shojaee, S. A.; Harriman, T. A.; Han, G. S.; Lee, J.-K.; Lucca, D. A. Substrate Effects on Photoluminescence and Low Temperature Phase Transition of Methylammonium Lead Iodide Hybrid Perovskite Thin Films. *Appl. Phys. Lett.* **2017**, *111*, 023902.
- (40) Sarang, S.; Ishihara, H.; Chen, Y.-C.; Lin, O.; Gopinathan, A.; Tung, V. C.; Ghosh, S. Low Temperature Excitonic Spectroscopy and Dynamics as a Probe of Quality in Hybrid Perovskite Thin Films. *Phys. Chem. Chem. Phys.* **2016**, *18*, 28428–28433.
- (41) Schmidt, T.; Lischka, K.; Zulehner, W. Excitation-Power Dependence of the near-Band-Edge Photoluminescence of Semiconductors. *Phys. Rev. B: Condens. Matter Mater. Phys.* **1992**, 45, 8989–8994.
- (42) Hoke, E. T.; Slotcavage, D. J.; Dohner, E. R.; Bowring, A. R.; Karunadasa, H. I.; McGehee, M. D. Reversible Photo-Induced Trap Formation in Mixed-Halide Hybrid Perovskites for Photovoltaics. *Chem. Sci.* **2015**, *6*, 613–617.
- (43) Slotcavage, D. J.; Karunadasa, H. I.; McGehee, M. D. Light-Induced Phase Segregation in Halide-Perovskite Absorbers. *ACS Energy Lett.* **2016**, *1*, 1199–1205.
- (44) Bischak, C. G.; Hetherington, C. L.; Wu, H.; Aloni, S.; Ogletree, D. F.; Limmer, D. T.; Ginsberg, N. S. Origin of Reversible Photoinduced Phase Separation in Hybrid Perovskites. *Nano Lett.* **2017**, *17*, 1028–1033.
- (45) Brennan, M. C.; Draguta, S.; Kamat, P. V.; Kuno, M. Light-Induced Anion Phase Segregation in Mixed Halide Perovskites. *ACS Energy Lett.* **2018**, *3*, 204–213.
- (46) Braly, I. L.; Stoddard, R. J.; Rajagopal, A.; Uhl, A. R.; Katahara, J. K.; Jen, A. K. Y.; Hillhouse, H. W. Current-Induced Phase Segregation in Mixed Halide Hybrid Perovskites and its Impact on Two-Terminal Tandem Solar Cell Design. *ACS Energy Lett.* **2017**, *2*, 1841–1847.
- (47) Beal, R. E.; Slotcavage, D. J.; Leijtens, T.; Bowring, A. R.; Belisle, R. A.; Nguyen, W. H.; Burkhard, G. F.; Hoke, E. T.; McGehee, M. D. Cesium Lead Halide Perovskites with Improved Stability for Tandem Solar Cells. *J. Phys. Chem. Lett.* **2016**, *7*, 746–751.
- (48) Draguta, S.; Sharia, O.; Yoon, S.; Brennan, M. C.; Morozov, Y. V.; Manser, J. S.; Kamat, P. V.; Schneider, W. F.; Kuno, M. Rationalizing the Light-Induced Phase Separation of Mixed Halide Organic-Inorganic Perovskites. *Nat. Commun.* **2017**, *8*, 200.
- (49) Li, W.; Rothmann, M. U.; Liu, A.; Wang, Z.; Zhang, Y.; Pascoe, A. R.; Lu, J.; Jiang, L.; Chen, Y.; Huang, F.; et al. Phase Segregation Enhanced Ion Movement in Efficient Inorganic CsPbIBr₂ Solar Cells. *Adv. Energy Mater.* **2017**, *7*, 1700946.
- (50) Vashishtha, P.; Halpert, J. E. Field-Driven Ion Migration and Color Instability in Red-Emitting Mixed-Halide Perovskite Nanocrystal Light-Emitting Diodes. *Chem. Mater.* **2017**, *29*, 5965–5973.
- (51) Hu, F.; Zhang, H.; Sun, C.; Yin, C.; Lv, B.; Zhang, C.; Yu, W. W.; Wang, X.; Zhang, Y.; Xiao, M. Superior Optical Properties of Perovskite Nanocrystals as Single Photon Emitters. *ACS Nano* **2015**, 9. 12410–12416.
- (52) Yoon, S. J.; Draguta, S.; Manser, J. S.; Sharia, O.; Schneider, W. F.; Kuno, M.; Kamat, P. V. Tracking Iodide and Bromide Ion Segregation in Mixed Halide Lead Perovskites during Photoirradiation. ACS Energy Lett. 2016, 1, 290–296.
- (53) Benavides-Garcia, M.; Balasubramanian, K. Bond Energies, Ionization Potentials, and the Singlet-Triplet Energy Separations of SnCl₂, SnBr₂, SnI₂, PbCl₂, PbBr₂, PbI₂, and their Positive Ions. *J. Chem. Phys.* **1994**, *100*, 2821–2830.
- (54) Haruyama, J.; Sodeyama, K.; Han, L.; Tateyama, Y. First-Principles Study of Ion Diffusion in Perovskite Solar Cell Sensitizers. *J. Am. Chem. Soc.* **2015**, *137*, 10048–10051.

- (55) Misra, R. K.; Aharon, S.; Li, B.; Mogilyansky, D.; Visoly-Fisher, I.; Etgar, L.; Katz, E. A. Temperature- and Component-Dependent Degradation of Perovskite Photovoltaic Materials Under Concentrated Sunlight. *J. Phys. Chem. Lett.* **2015**, *6*, 326–330.
- (56) Yoon, S. J.; Stamplecoskie, K. G.; Kamat, P. V. How Lead Halide Complex Chemistry Dictates the Composition of Mixed Halide Perovskites. *J. Phys. Chem. Lett.* **2016**, *7*, 1368–1373.
- (57) Ruess, R.; Benfer, F.; Böcher, F.; Stumpp, M.; Schlettwein, D. Stabilization of Organic-Inorganic Perovskite Layers by Partial Substitution of Iodide by Bromide in Methylammonium Lead Iodide. *ChemPhysChem* **2016**, *17*, 1505–1511.
- (58) Zhang, H.; Fu, X.; Tang, Y.; Wang, H.; Zhang, C.; Yu, W. W.; Wang, X.; Zhang, Y.; Xiao, M. Phase Segregation due to Ion Migration in All-Inorganic Mixed-Halide Perovskite Nanocrystals. *Nat. Commun.* **2019**, *10*, 1088.
- (59) Hoffman, J. B.; Schleper, A. L.; Kamat, P. V. Transformation of Sintered CsPbBr₃ Nanocrystals to Cubic CsPbI₃ and Gradient CsPbBr_xI_{3-x} through Halide Exchange. *J. Am. Chem. Soc.* **2016**, *138*, 8603-8611.